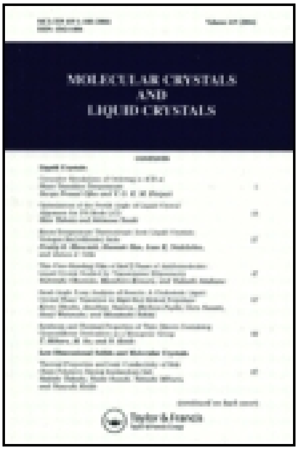

Molecular Crystals and Liquid Crystals
Publication details, including instructions for authors and subscription information:
http://www.tandfonline.com/loi/gmcl20

Designing Liquid Crystalline Nonlinear Optical Meta-materials with Large Birefringence and Sub-unity Refractive Index

I. C. Khoo [a], D. H. Werner [a], D. H. Kwon [a] & A. Diaz [a]

[a] Electrical Engineering Department, The Pennsylvania State University, University Park, PA, USA

Version of record first published: 22 Sep 2010

Mol. Cryst. Liq. Cryst., Vol. 488, pp. 88–99, 2008

ISSN: 1542-1406 print/1563-5287 online
DOI: 10.1080/15421400802240318

Designing Liquid Crystalline Nonlinear Optical Meta-materials with Large Birefringence and Sub-unity Refractive Index

I. C. Khoo, D. H. Werner, D. H. Kwon, and A. Diaz
Electrical Engineering Department, The Pennsylvania State University, University Park, PA, USA

We describe here two types of liquid crystalline meta-materials which exhibit large birefringence and sub-unity or negative refractive index. The conditions on the constituents' complex permittivity and permeability for producing effective refractive indices in this unconventional range are explicitly illustrated with two exemplary liquid crystalline meta-materials: (i) core-shell nano-spheres randomly dispersed in a nematic liquid crystal and (ii) planar nano-structures juxtaposed with a layer of liquid crystal. Both systems also exhibit enhanced electro-optical and nonlinear optical responses. These meta-materials may find applications in the next generation reflective, transmissive, modulation and switching elements and devices in the visible–infrared–Terahertz and microwave regimes.

Keywords: electro-optics; nonlinear optics; large birefringence; liquid crystal meta-materials; sub-unity and negative refractive index

I. INTRODUCTION

Nematic liquid crystals (NLC) are widely studied in the last two decades for their extraordinary nonlinear and electro-optical responses, as a result of their large birefringence and the easy susceptibility of the crystalline axis to reorientation by external fields [1–25]. By considering the free energy involved in the reorientation [1], it has been shown that the director axis deformation/reorientation induced refractive index change experienced by an extraordinary-polarized light is $\Delta n \sim \eta(n_e - n_o)\ \mathrm{I}\tau\ \alpha\Lambda^2/\mathrm{K}$, where K is the LC elastic constant,

This work is supported by the National Science foundation, the Air Force Office of Scientific Research and the Army Research Office.

Address correspondence to I. C. Khoo, Pennsylvania State University, Electrical Engineering Department, University Park, PA 16802, USA. E-mail: ick1@psu.edu

Λ is the characteristic length for the distortion, η is conversion efficiency of light energy to reorientation, τ the response time of the reorientation process, I the optical intensity and α is the loss coefficient due to the transfer of energy from light to nematic reorientation per unit length. Writing $\Delta n = n_2 I$ yields the nonlinear index coefficient n_2, which is often also referred to as the optical nonlinearity:

$$n_2 \sim \eta(n_e - n_o)\tau\ \alpha\Lambda^2/K\pi^2. \tag{1}$$

From (1), and using $n_2 = 0.105\chi^{(3)}_{cgs}/n^2\,[\mathrm{cm}^2/\mathrm{Watt}]$ [1], where $\chi^{(3)}$ is the third order nonlinear susceptibility, we can define a Figure of Merit (FOM) for the optical nonlinearity

$$\mathrm{FOM} = \chi^{(3)}/\tau\alpha \sim \eta(n_e - n_o)\ n_o^2\ n^2\Lambda^2/K \tag{2}$$

For nematic liquid crystals [1], typical τ is $\sim 10^{-2}$ s for $\Lambda \sim 20\,\mu$m. Using $K \sim 10^{-7}$ erg/cm, $(n_e - n_o) \sim 0.2, \alpha \sim 100\,\mathrm{cm}^{-1}$, we have $n_2 \sim 1\,\mathrm{cm}^2/\mathrm{W}$ [3,13,18]. To date, n_2 values approaching $1000\,\mathrm{cm}^2/\mathrm{W}$ have been observed [10]. In contrast to what used to be regarded as a highly nonlinear anisotropic fluid such as CS_2 which possesses a nonlinearity on the order of $10^{-10}\,\mathrm{cm}^2/\mathrm{W}$, these supra nonlinear nematic liquid crystalline (NLC) systems have ushered in the era of nonlinear optics with μW and nW threshold powers [25] and compact device size and dimensions.

These NLC nonlinearities and the Figure of Merit $[\chi^{(3)}/\tau\alpha]$ are listed in Tables 1 and 2 together with other classes of materials [semiconductors and polymers] in which large optical nonlinearities have also been observed [17–22]. In contrast to other material nonlinearities that are generally narrow-band (centered around some electronic resonances), an unique feature of NLC nonlinearity is that it is extremely broadband, as the underpinning mechanism of laser induced director axis

TABLE 1 Refractive Index Coefficients of Some Nonlinear Optical Materials

Materials	Order of magnitude of n_2 (cm^2/W)
Nematic Liquid Crystal	
Photorefractive -C60 doped [13]	10^{-3}
Photorefractive-methyl-red doped [3]	>1
C60/nanotube doped nematic [13]	$\sim 10^{-1}$
GaAs bulk [26]	10^{-5}
GaAs MQW [27]	10^{-3}
GaAs MQW [27]	10^{-3}
Photorefractive crystals/polymers [28]	10^{-4}
Bacteriorhodopsin [29]	10^{-3}

TABLE 2 Switching Efficiency $\chi^{(3)}/\alpha\tau$ of Various Materials

Materials	$\chi^{(3)}/\alpha\tau$ ($10^{-10}\,m^3\,V^{-2}\,s^{-1}$)
Methyl-red doped LC film	200
C60/nanotube doped film	$\sim$ 500
GaAs bulk	30
GaAs MQW	300
Bacteriorhodopsin	0.05

Note: $n_2 = 0.105 \times \chi^{(3)}_{cgs}\ /n^2$ [cm^2/Watt]; $\chi^{(3)}$ [in m^2/V^2) $= 1.39\times\ 10^{-8}\ \chi^{(3)}_{cgs}$ [in esu]. For MRNLC, $\alpha = 150\,cm^{-1}$, response time $\tau = 10\,ms, \chi^{(3)} = 3.13 \times 10^{-6}$ (m^2/V^2), *so* $\chi^{(3)}/\alpha\tau = 209$ ($10^{-10}\,m^3\,V^{-2}\,s^{-1}$).

reorientation is a non-resonant process dictated mostly by the birefringence ($n_e - n_o$). For nematic liquid crystals, $(n_e - n_o) \sim 0.2$ to 0.6, which ranks as the largest of all known materials and more importantly, the large birefringence spans the entire visible, through the infrared IR to longer wavelengths [1]. We discuss here two approaches to realize liquid crystalline materials possessing large birefringence, and therefore enhanced nonlinear optical responses: (a) random distribution of nano-particulates in aligned NLC host and (b) juxtaposition a layer of NLC to planar nano-structures. In both cases, the method involves judicious choice of the constituents' permittivity ε and permeability μ to create meta-materials of desired effective complex dielectric constants ε_{eff} [and therefore the complex refractive indices and birefringence].

II. SUB-UNITY AND NEGATIVE REFRACTIVE INDEX DESIGN GUIDELINES – PERMITTIVITY AND PERMEABILITY PARAMTERS

Considering the fact that the refractive index of vacuum is unity, one can envision from basic electromagnetic considerations that materials that possess sub-unity ($n < 1$), zero ($n = 0$) or negative ($n < 0$) refractive index will have many reflective and transmissive properties otherwise not possible with conventional materials ($n > 1$). In recent years, these so-called meta-materials have received intense interests and many actual demonstrations of materials with sub-unity and negative index have been reported [22–24,30–35]. Nevertheless, the conditions for achieving such unconventional refractive indices in meta-materials are not very well documented. We present here explicit expressions and illustrations based on basic electromagnetic considerations.

The derivation of the conditions and the analysis of the material behavior as a function of a given parameter (such as the refractive index of the nematic liquid crystal constituent) are simplified by defining a normalized permittivity and permeability (and associated angles) in terms of the relative permittivity and permeability ε_r and μ_r as:

$$\varepsilon'_N + i\varepsilon''_N = \frac{\varepsilon'_r}{|\varepsilon_r|} + i\frac{\varepsilon''_r}{|\varepsilon_r|} \equiv \cos\theta_\varepsilon + i\sin\theta_\varepsilon \tag{3a}$$

$$\mu'_N + i\mu''_N = \frac{\mu'_r}{|\mu_r|} + i\frac{\mu''_r}{|\mu_r|} \equiv \cos\theta_\mu + i\sin\theta_\mu \tag{3b}$$

The angles θ_ε and θ_μ are defined in the interval $(-\pi, \pi]$. The normalized refractive index is similarly defined as:

$$n_N = \pm\sqrt{\varepsilon_N\mu_N} = \pm\exp\left(i\frac{\theta_\varepsilon+\theta_\mu}{2}\right) = \exp\left(i\frac{\theta_\varepsilon+\theta_\mu}{2} + im\pi\right) = n'_N + in''_N \tag{3c}$$

If we consider a wave propagating in the positive z direction, the appropriate sign (or value of m equal to zero or one) is chosen so that power flow in the $+z$ direction is positive. This condition implies choosing the sign so that

$$\pm\cos\left(\frac{\theta_\varepsilon-\theta_\mu}{2}\right) > 0 \tag{4}$$

If the wave propagates in the $-z$ direction, the opposite root should be taken. The power flow requirement implies also that the impedance $\eta = \frac{\mu_r}{n}\eta_0$ is always positive. Hence the impedance can always be defined as (the positive square root) $\eta = \sqrt{\frac{\mu}{\varepsilon}}$. The refractive index n can then be expressed as:

$$\begin{aligned} n &= \operatorname{sign}\left(\cos\left(\frac{\theta_\varepsilon-\theta_\mu}{2}\right)\cos\left(\frac{\theta_\varepsilon+\theta_\mu}{2}\right)\right)\sqrt{\varepsilon_r\mu_r} \\ &= \operatorname{sign}\left(\cos\theta_\varepsilon + \cos\theta_\mu\right)\sqrt{\varepsilon_r\mu_r} \end{aligned} \tag{5}$$

where it is understood the positive square root is to be taken. The sign of the refractive index is therefore given by $\operatorname{sign}\left(\cos\theta_\varepsilon + \cos\theta_\mu\right)$.

It is now useful to consider the real and imaginary parts of the normalized refractive index as a function of the permittivity and permeability angles θ_ε and θ_μ. The real and imaginary parts of the normalized refractive index are plotted below in Figure 1. Negative index behavior ($\mathrm{Re}\{n\} < 0$) is shown in black in Figure 1a and correspond to negative values in the adjacent 3D plot. The condition for negative

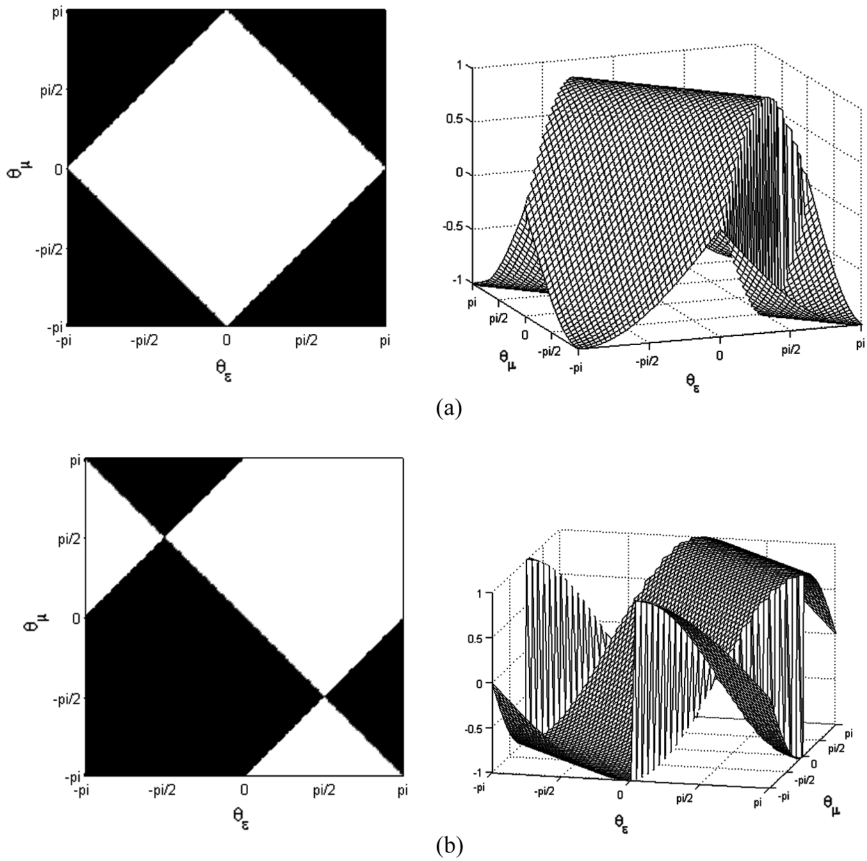

FIGURE 1 (a) Regions in phase space $\theta_\varepsilon\theta_\mu$ of positive index (white) and negative index (black) behavior and 3-D plot of the real part of the normalized refractive index (n'_N). (b) Regions in phase space $\theta_\varepsilon\theta_\mu$ where the material is lossy (white) or exhibits gain (black) and 3-D plot of the imaginary part of the normalized refractive index (n''_N).

index ($\cos(\theta_\varepsilon) + \cos(\theta_\mu) < 0$) is commonly found in the literature as the equivalent expression: $\varepsilon'|\mu| + \mu'|\varepsilon| < 0$. This expression is totally general and works even if the material exhibits gain. Figure 1b shows the regions where the material is lossy (in white) or where it exhibits gain (in black).

We now apply these conditions on the complex material permittivity and permeability to design liquid crystalline meta-materials of desired refractive indices in the sub-unity to negative range.

III. A. DISPERSION OF NANOPARTICLES IN NEMATIC LIQUID CRYSTALS

In approach I, nano-spheres [core-shell or single constituent made of metals (Drude-type or plasmonic) or semiconductors are dispersed in aligned nematic liquid crystals as depicted in Figure 2. The size of the nano-spheres is much smaller than the optical wavelength, and therefore the incident light 'sees' an effective refractive index which can be calculated using the effective medium theory [36]. We have performed several calculations for a variety of nano-spheres in various combinations and liquid crystal alignments, including (i) Polaritonic-Drude (core-shell) nano-spheres and (ii) Gold-coated silica spheres.

Consider the case of core-shell nano-spheres, for example. The permittivity of a polaritonic core [22,37–39] is of the form $\varepsilon_1 = \varepsilon(\infty)\left(1 + \frac{\omega_L^2 - \omega_T^2}{\omega_T^2 - \omega^2 - i\omega\gamma_1}\right)$ where $\varepsilon(\infty)$ is the high-frequency limit of the permittivity, ω is the incident frequency, ω_T is the transverse optical phonon frequency, ω_L is the longitudinal optical phonon frequency, and γ_1 is the damping coefficient. On the other hand, the Drude [39] shell's permittivity is given by $\varepsilon_2 = 1 - \frac{\omega_p^2}{\omega^2 + i\omega\gamma_2}$where ω_p is the plasma frequency and γ_2 is the damping term. The optical permittivity of the host nematic liquid crystal (NLC) for a linearly polarized light incident at an oblique angle θ is given by $\varepsilon_3 = \frac{\varepsilon_e \varepsilon_o}{\varepsilon_e \cos^2\theta + \varepsilon_o \sin^2\theta}$ where ε_e and ε_o are the respective permittivities for light polarized parallel and perpendicular to the director axis $\hat{n}$, and θ is the angle made by the director axis with the optical wave vector k_0.

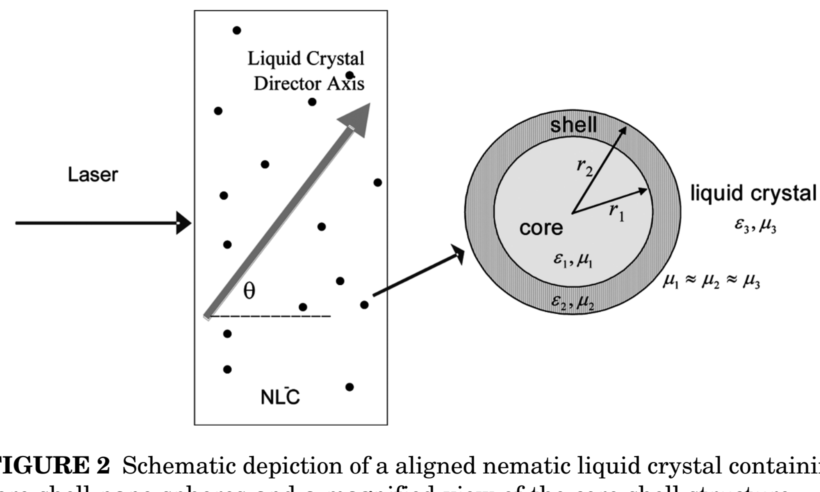

FIGURE 2 Schematic depiction of a aligned nematic liquid crystal containing core-shell nano-spheres and a magnified view of the core-shell structure.

Using the Maxwell Garnet mixing rule [22], the effective permittivity and permeability ε_r^{eff} and μ_r^{eff} for NDLC can be calculated to give respectively by:

$$\varepsilon_r^{eff} = \varepsilon_3\left(\frac{k_3^3 + j4\pi N a_1}{k_3^3 - j2\pi N a_1}\right) \tag{6}$$

$$\mu_r^{eff} = \frac{k_3^3 + j4\pi N b_1}{k_3^3 - j2\pi N b_1} \tag{7}$$

where

$$k_3 = \sqrt{\varepsilon_3}k_0 = \left(\frac{\varepsilon_e\varepsilon_o}{\varepsilon_e\cos^2\theta + \varepsilon_o\sin^2\theta}\right)^{1/2} k_0 \tag{8}$$

and a_1 and b_1 are the MIE scattering coefficients of the coated dielectric sphere [31], N is the volume density of the spheres $(N = 3f/4\pi r_2^3)$ and f is the filling fraction of the composite.

Figure 3 shows an exemplary results for a filling fraction $f = 0.1$, $r_1 =\ 0.13\,\mu\text{m}$, $r_2 = 0.143\,\mu\text{m}$ *and* the following parameters for the constituent core, shell and host: $\varepsilon(\infty) = 17$, $\omega_L/2\pi = 570$ THz, $\omega_T/2\pi = 240\,\text{THz}$, $\gamma_1/2\pi = 2.5\,\text{THz}$, $\mu_1 = \mu_2 = \mu_3 = 1$, $\gamma_2\ = \omega_p/60$, $\omega_p/2\pi = 134.0\,\text{THz}$ and the LC birefringence $\Delta n_{\text{LC}} = n_e - n_o \sim 0.6$, corresponding to the nematic host dielectric anisotropy of $\varepsilon_e - \varepsilon_o = 2$; $\varepsilon_e \sim 4$ and $\varepsilon_0 \sim 2$. Such liquid crystalline meta-materials, by virtue of having these high-dielectric-constant constituent nano-spheres, generally possess larger effective birefringence than the liquid crystal 'host', although in general they are also more absorptive due to the larger value of the imaginary part of the n_{eff}. Nevertheless, there are regions where the absorption is low, e.g. around 50–70 THz region. In this regime the effective birefringence Δn_{eff} is ~ 0.75 [at 50 THz] or 0.9 [at 70 THz], compared to $\Delta n_{\text{LC}} = n_e - n_o \sim 0.6$. At 80 THz, where the loss is still low, the effective birefringence is as large as ~ 1.1. An even more interesting property of such core-shell nano-sphere doped liquid crystal is that in some frequency interval [around 107 THz], the effective refractive index can assume sub-unity (< 1), zero or negative (< 0) values as the dielectric constant of the host nematic liquid crystal is changed, but accompanied by relatively high loss (larger values of the imaginary part of n_{eff}. The challenge in the material design, therefore, is to search and identify regions in the effective μ-ε space, c.f. Figure 1 whereby the desired index value [both real and imaginary part] can be attained.

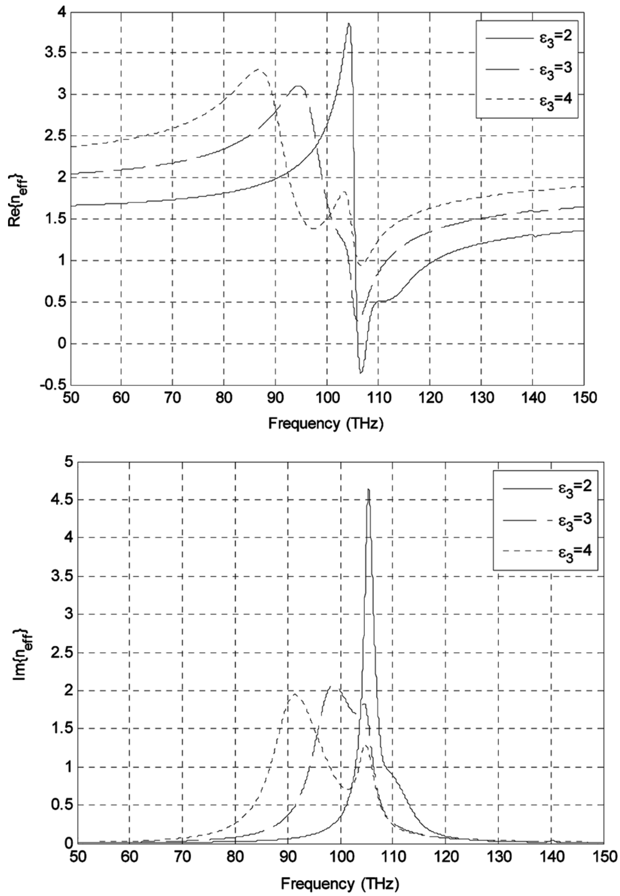

FIGURE 3 Real part Re$\{n_{eff}\}$ and Imaginary part Im$\{n_{eff}\}$ of the complex effective refractive index $\{n_{eff}\}$ of the nano-spheres-dispersed NLC in the 50–150 tHz region. The dimensions and composition of the spheres can be scaled up/down for applications in other spectral region.

III.B. PLANAR NANOSTRUCTURES CONTAINING A NEMATIC LIQUID CRYSTAL LAYER

The other meta-material approach we employed is to infiltrate liquid crystal in nano-structures such as such as frequency selective surfaces [19,23–24,40–41], some of which also exhibit tunable refractive indices from negative through zero to positive values. Frequency selective surfaces are 2D periodic arrays of cells, where each cell consists of metallic patches or apertures (in metallo-dielectric FSSs) or in a patterned configuration of two dielectrics with different optical properties (in the case of all-dielectric FSSs). Their use in the visible-IR region stems from the FSS concept in the microwave regime, since frequency response scales with element dimensions. Depending on the cell pattern, size, and constituent materials, these FSS could function as total reflection or transmission devices, low-pass, band-pass,

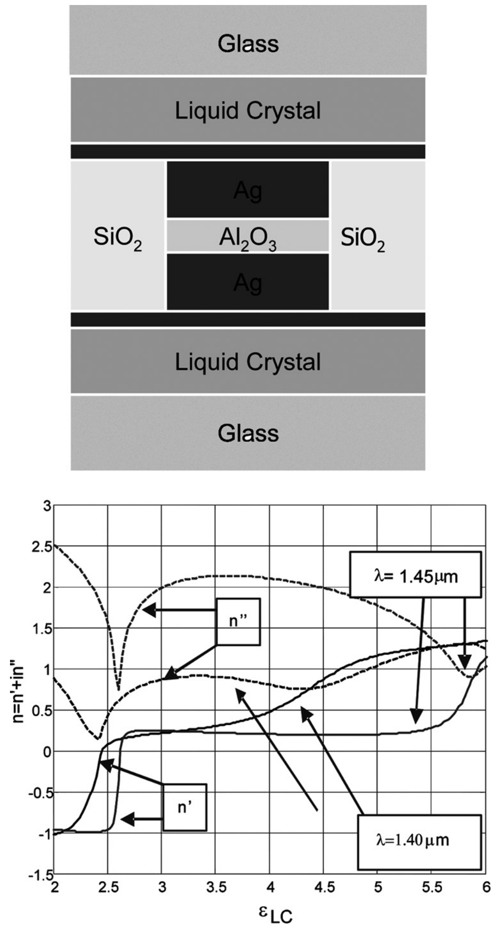

FIGURE 4 Schematic depiction of a unit cell in the liquid crystal clad metallo-dielectric nano-structured meta-material (upper figure) and plots of the effective real [n'] and imaginary [n''] part of the complex refractive index for various values of the liquid crystal dielectric constant and two laser wavelengths.

notch-, high-pass, and multi-band- filters. By incorporating a tunable material constituent such as liquid crystals, one can impart tunability in these FSS's as demonstrated in recent articles [19,23–24].

We have recently reported another liquid crystal meta-material nanostructure formed by periodic arrays of unit cells which are made up of magnetic resonator and negative dielectric constant material in juxtaposition with aligned nematic liquid crystal. An exemplary nanostructure is depicted in Figure 4. It consists of two aligned nematic liquid crystal layers sandwiching a FSS-like metallo-dielectric nanostructure. The unit cell of the FSS nano-structure comprises a magnetic resonator made of two strips of silver of thickness 30 nm separated by a thin layer of alumina of thickness 20 nm. Negative permittivity needed for negative-index behavior is provided by thin silver films bounding the periodic array of magnetic resonators. The space between neighboring magnetic resonators is filled with silica. Figure 4 also shows some exemplary plots of the effective refractive indices of these meta-materials as a function of the liquid crystal's dielectric constant for two optical wavelengths (1.40 μm and 1.45 μm). The lower right solid curve for incident light wavelength $\lambda = 1.45\,\mu\text{m}$, for instance, shows that the real part of the effective refractive index changes by a substantial amount of 1.3 [from -1 to 0.3] as the LC dielectric constant is tuned from 2.5 to 2.75 (index change of 0.07 from 1.58 to 1.65). Similar dramatic changes also arise for the $\lambda = 1.40\,\mu\text{m}$ case; the real part of the nanostructure's refractive index changes by ~ 1.1 (from -1 to 0.1) as the LC dielectric constant is (optically) tuned from 2 to 2.5 [LC index change of from 1.41 to 1.58]. In other words, these liquid crystalline nano-structured metamaterials, similar to the nano-sphere doped liquid crystals discussed in the preceding sections, possess much higher birefringence than the nematic constituent, and also exhibit unconventional refractive index values in the sub-unity to negative range.

IV. CONCLUSION

In conclusion, we have provided a brief overview of progresses in the studies of liquid crystal nonlinear optics response due to director axis reorientation, and recent efforts to develop liquid crystalline materials having large birefringence and unconventional refractive indices in the sub-unity and below-zero ranges. We presented the design guidelines for realizing such meta-materials with unconventional refractive index and described two examples of liquid crystalline meta-materials with such properties. Both approaches have their advantages and limitations. In the case of nano-dispersions, the large filling factor

($\sim$10%) requirement may cause serious order parameter perturbation on the liquid crystalline host, whereas the planar nano-structures would require complex nano-fabrication procedures [42,43]. In both cases, nevertheless, the meta-material designs can be scaled for application over a very broad spectral range [from visible through infrared to the Terahertz regimes]. By virtue of the nematic constituents, the effective refractive indices of these meta-materials can also be tuned by electrical, optical or temperature means.

REFERENCES

[1] Khoo, I. C. (2007). *Liquid Crystals*, 2nd, Wiley: NJ.
[2] Tondiglia, V. P., Natarajan, L., Sutherland, R. L., Tomlin, D., & Bunning, R. J. (2002). *Adv. Mater.*, *14*(3), 187–191 and references therein.
[3] Khoo, I. C., Slussarenko, S., Guenther, B. D., & Wood, W. V., (1998). *Opt. Letts.*, *23*, 253–255.
[4] Kaczmarek, Malgosia, Shih, Min-Yi, Cidney, Roger, S., & Khoo, I. C. (2002). *IEEE J. Quantum Electronics*, *38*, 451–457.
[5] Khoo, I. C. (1983). *Phys. Rev.*, *A27*, 2747.
[6] Khoo, I. C. (1982). *Appl. Phys. Letts.*, *40*, 645.
[7] Khoo, I. C. & Shepard, S. (1983). *J. of Appl. Phys.*, *54*, 5491.
[8] Khoo, I. C. & Normandin, R. (1984). *Opt. Letts.*, *9*, 285–287.
[9] Khoo, I. C. Lindquist, R. G., Michael, R. R., Mansfield, R. J., & Lopresti, P. (1991). *J. Appl. Phys.*, *69*, 3853.
[10] Lucchetti, L., Fabrizio, M. Di., Francescangeli, O., & Simoni, F. (2004). *Opt. Comm.*, *233*, 417.
[11] Khoo, I. C. (1996). *IEEE J. Quant. Elect.*, *32*, 525–534.
[12] Khoo, I. C., Li, H., & Liang, Y. (1994). *Opt. Lett.*, *19*, 1723–1725.
[13] Khoo, I. C., Ding, J., Zhang, Y., Chen, K., & Diaz, A. (2003). *Appl. Phys. Letts.*, *82*, 3587–3589.
[14] Khoo, I. C., Chen, Kan, & Williams, Y. Zhang, (2006). *IEEE J. Selcted Topics in Quantum Electronics JSTQE*, *2*(3), 443–450.
[15] Buchnev, O., Dyadyusha, A., Kaczmarek, M., Reshetnyak, V., & Reznikov, Y. (2007). *J. Opt. Soc. Am.*, *B 24*(7), 1512–1516.
[16] See for example, Tabiryan, N. V., & Umeton, C. (1998). *J. Opt. Soc. Am.*, *B15*, 1912–1917.
[17] Kaczmarek, Malgosia, Dyaduysha, Andrey, Slussarenko, Sergei, & Khoo, I.C. (2004). *J. Appl. Phys.*, *96*, 2616–2623.
[18] Khoo, I. C., Shih, Min-Yi, Wood, M. V., Guenther, B. D., Chen, P. H., Simoni, F., Slussarenko*, S., Francescangeli, O., & Lucchetti, L. (1999). *IEEE Proceedings*, *87*(11), 1897–1911.
[19] Khoo, I. C., Williams, Yana, Diaz, Andres, Chen, Kan, Bossard, J., Werner, D., Graugnard, E., & Summers, C. J. (2006). *Molecular Crystal Liquid Crystal*, *453*, 309–319.
[20] Kubo, Shoichi, Diaz, Andres, Tang, Yan, Mayer, Theresa S., Khoo, I. C., & Mallouk, Thomas E. (2007). *Nanoletters*, *7*, 3418–3423.
[21] Graugnard, E., King, J. S., Jain, S., Summers, C. J., Zhang-Williams, Y., & Khoo, I. C. (2005). *Phys. Rev.*, *B72*, 233105.

[22] Khoo, I. C., Werner, D. H., Liang, X., Diaz, A., & Weiner, B. (2006). *Optics Letts.*, *31*, 2592.
[23] Werner, D. H., Kwon, D-H., Khoo, I. C., Kildeshev, A. K., & Shalaev, V. M. (2007). *Optics Express*, *15*(6), 3342–3347.
[24] Wang, Xiande, Kwon, Do-Hoon, Werner, Douglas H., Khoo, Iam-Choon, Kildishev, Alexander V., & Shalaev, Vladimir M. (2007). *Appl. Phys. Lett.*, *91*, 143122 (3 pages).
[25] Khoo, I. C., Wood, M. V., Shih, M. Y., & Chen, P. H. (1999). *Optics Express*, *4*(11), 431–442.
[26] Oudar, J. L. (1986). In: *Nonlinear Optics Materials and Devices*, Flytzanis, C., & Oudar, J. L. (Eds.), Springer: Berlin, p. 91.
[27] Chemla, D. S. (1986). In: *Nonlinear Optics Materials and Devices*, Flytzanis, C., & Oudar, J. L. (Ed.), Springer: Berlin, p. 65.
[28] Moerner, W. E., & Silence, S. M. (1994). *Polymeric Photorefractive Materials*, Chemical reviews 94, 127–155. See also reference 1.
[29] Thoma, R., Hampp, N., Brauchle, C., & Oesterhelt, D. (1991). *Opt. Lett.*, *16*, 651.
[30] Moussa, R., Foteinopoulou, S., Zhang, L., Tuttle, G., Guven, K., Ozbay, E., & Soukoulis, C. M. (2005). *Phys Rev.*, *B71*, 85106.
[31] Martínez, A., & Martí, J. (2005). *Phys. Rev.*, *B71*, 235115.
[32] Bulu, I., Caglayan, H., & Ozbay, E. (2005). *Phys. Rev.*, *B72*, 045124.
[33] Zhang, X. (2005). Subwavelength far-field resolution in a square two-dimensional photonic crystal. *Phys. Rev.*, *E71*, 037601.
[34] Schonbrun, E., Tinker, M., Park, W., & Lee, J.-B. (2005). *IEEE Photon. Technol. Lett.*, *17*, 1196–1198.
[35] Podolskiy, V. A., Sarychev, A. K., & Shalaev, V. M. (2003). *Optics Express*, *11*, 735–745.
[36] Bohren, C. F., & Huffman, D. R. (2004). *Absorption and Scattering of Light by Small Particles*, Wiley-VCH.
[37] Schall, M., Helm, H., & Keiding, S. R. (1999). *Int. J. Infrared Millimeter Waves*, *20*, 595.
[38] Wheeler, M. S., Aitchison, J. S., & Mojahedi, M. (2006). *Phys. Rev.*, *B73*, 045105.
[39] Rakic, A. D., Djurisic, A. B., Elazar, J. M., & Majewski, M. L. (1998). *Applied Optics*, *37*, 5271–5283.
[40] Wu, T. K. (1995). *Frequency Selective Surface and Grid Array*, Wiley & Sons: New York.
[41] Bossard, J. A., Liang, X., Li, L., Werner, D. H., Weiner, B., Cristman, P. F., Diaz, A., & Khoo, I. C. (2008). *IEEE Transactions on Antennas and Propagation*, *56*, 1308–1320.
[42] Diviliansky, Ivan B., Shishido, Atsushi, Khoo, I. C., Mayer, Theresa S., Pena, David, Nishimura, Suzushi, & Mallouk, Thomas E. (2001). *Appl. Phys. Letts.*, *79*, 3392–3394.
[43] Shishido, Atsushi, Diviliansky, Ivan B., Khoo, I. C., Mayer, Theresa S., Nishimura, Suzushi, Egan, Gina L., & Mallouk, Thomas E. (2001). *Appl. Phys. Letts.*, *79*, 3332–3334.